Submillimeter Cyclotron Resonance and Related Phenomena in HgTe

J. Tuchendler, M. Grynberg,* Y. Couder, H. Thomé, and R. Le Toullec†
Laboratoire de Physique des Solides de l'Ecole Normale Supérieure, 24 Rue Lhomond, Paris V^e, France
(Received 7 March 1973)

We present the results of far-infrared magnetotransmission experiments on mercury telluride. The experiments are performed on n-type samples in the Faraday and Voigt geometries in the wavelength range from 2 mm to 100 μm at 4.2 K and in magnetic fields up to 58 kG. Both intraband transitions in the Γ_8 conduction band, such as cyclotron resonance, and interband $\Gamma_8 \rightarrow \Gamma_8$ transitions are observed: To analyze the position of the plasma-cylotron-resonance line observed in the Voigt geometry, we discuss the frequency and magnetic field dependence of all the contributions to the dielectric function including that which arises from the interband $\Gamma_8 \rightarrow \Gamma_8$ transitions. The Luttinger parameters γ_1, $\bar{\gamma}$, and κ describing the quantum levels in the Γ_8 bands near the degeneracy point at $\vec{k} = 0$ are determined. Absorption lines due to transitions between a discrete acceptor state degenerate with the conduction band and the quantum levels of the conduction band are observed. The activation energy of this acceptor state is found to be $E_A = 0.7 \pm 0.1$ meV.

I. INTRODUCTION

The zero-gap band structure of mercury telluride (Fig. 1) yields a number of specific problems. Magnetotransmission through a sample at submillimeter frequencies gives direct information on these special features.

(i) Owing to the degeneracy of the top of the Γ_8 valence band with the bottom of the Γ_8 conduction band, there is a mixing of the wave functions of the electrons and holes near $\vec{k} = 0$. In this case, the quantum energy levels in the Γ_8 bands in the presence of a magnetic field are unevenly spaced for low quantum numbers. Then, the knowledge of the effective mass and the Landé factor, sufficient to describe the levels in the high-quantum-number limit, is meaningless. The low-quantum-number levels are described by the parameters introduced by Luttinger[1] to interpret the quantum effects observed by Fletcher *et al.*[2] in the cyclotron-resonance transition on p-type germanium. The absorption lines observed in our energy range are related to intraband and interband transitions between energy levels close to the Γ_8 point. Taking into account the results of magnetotransmission experiments in the near-infrared region, we obtain the values of the Luttinger parameters and a complete description of the quantum levels.

(ii) The frequency dependence of the dielectric function is different from what it is in a usual semiconductor with a finite energy gap. The contribution to the dielectric function of the $\Gamma_8 \rightarrow \Gamma_8$ interband transitions depends strongly on the relative amplitude of the photon energy and of the Fermi energy, as was shown by Sherrington and Kohn,[3] Broerman,[4] and Grynberg, Le Toullec, and Balkanski.[5] This effect must be taken into account when studying magnetoplasma phenomena. In particular, the theory of the magnetoplasma cyclotron resonance in the Voigt configuration must be modified. We have calculated the positions of this resonance, at a given photon energy, as a function of magnetic field. The observed position is in very good agreement with the theoretical predictions.

(iii) What is the structure of the impurity levels in such a material? This problem has been recently discussed theoretically by Gel'mont and D'yakonov.[6] We observe absorption lines which we relate to the presence of impurities giving rise to discrete acceptor states degenerate with the conduction-band continuum.

II. EXPERIMENTAL DETAILS

A. Sample Preparation and Handling

The samples used in our experiments were obtained according to the following procedure. A solution of 0.5 at.% of tellurium in mercury is heated up to 500 °C in a quartz ampulla and cooled to room temperature in a 6-day operation. A thin monocrystalline layer floats on the mercury surface. The thickness of the layer varies from 20 to 80 μm. Its surfaces are (111) planes. Samples from such a layer are chemically etched in a solution of 5 at.% of bromine in methylic alcohol. The thickness is reduced to less than 10 μm. These samples are n type. The free-electron concentration and the mobility at 4.2 K, deduced from Hall measurements on similar samples 60 μm thick, are around 2×10^{15} cm^{-3} and 6×10^{5} cm^{2}V^{-1} sec^{-1}, respectively.

The sample is then placed between two disks of brass with a hole pierced in their centers. A thin indium ring surrounds the sample between the two disks, and the disks are pressed together until their distance hardly exceeds the thickness of the sample [Fig. 2(b)]. This "sandwich" is glued in

one of the experimental positions sketched in Figs. 2(a) and 2(c).

B. Microwave Sources

The experiments were performed at 4.2 K in a large energy range. We used two types of microwave sources: six backward-wave oscillators, "carcinotrons",[7] emitting, respectively, in the wavelength range 2 mm, 1 mm, 900 μm, 700 μm, 600 μm, 500 μm, and two molecular gas lasers operated on the following lines: 337 and 311 μm with HCN, 195 μm with DCN, and 118 μm with H_2O. Thus we could work at photon energies from 0.5 meV up to 10.5 meV. The output power of the sources ranges from several milliwatts to a few watts. Consequently, attenuation is required in all cases to prevent the destruction of the samples, which could be due to the strains of overheating. The amplitude of the power emitted by the sources at a given wavelength is modulated electronically at any frequency between 10 and 400 Hz in order to use a lock-in amplifier. To do this, when using a carcinotron, one modulates the intensity of the electron beam by adding an ac voltage to the anode voltage. In the case of the lasers this is achieved by modulation of the intensity of the current in the discharge.

C. Experimental Arrangement

From the source to the sample, the far-infrared radiation is propagated in oversized waveguides and light pipes. Conventional attenuators of 4-mm radiation are used with the carcinotrons, and Mylar sheets of different thicknesses with the lasers.

The experiments are performed in the axial magnetic field of a superconducting coil. The magnetic field can be continuously swept up to 58 kG. A sketch of the various experimental arrangements is shown in Fig. 2. The light received from the source is reflected by a mirror at 45°. It propagates towards the sample along a stainless-steel light pipe, 8 mm in diameter.

For the experiments performed in the Faraday geometry, the sample holder is glued on the part shown in Fig. 2(c), which is placed at the end of the light pipe. For the experiments in the Voigt configuration [Fig. 2(a)] a mirror at 45° reflects the microwave, which is directed onto the sample placed in a vertical plane. In front of the sample, a unidirectional grid linearly polarizes the incident wave. The electric field associated to the microwave can be set either perpendicular to or parallel to the static magnetic field.

The microwave energy transmitted through the sample is detected by a bolometer placed behind the sample. We use a carbon bolometer which is a regular Allen-Bradley resistor (100 Ω, $\frac{1}{10}$ W). The resistor is thinned down to about 0.2 mm, and has a parallelepiped shape. It is glued on a brass support, from which it is electrically isolated by a Mylar sheet. The bottom of the waveguide, and the sample holder, are located in a chamber sealed with Wood's metal, which can be filled with an exchange gas.

III. RESULTS AND INTERPRETATION

We present in Figs. 3, 4, and 5 some experimental recordings obtained at various wavelengths for the Faraday geometry ($\vec{q} \parallel \vec{B}_0$) (in Fig. 3), the Voigt geometry ($\vec{q} \perp \vec{B}_0 \perp \vec{E}$) (in Fig. 4), and the Voigt geometry ($\vec{q} \perp \vec{B}_0 \parallel \vec{E}$) (in Fig. 5).

The most evident feature of these recordings is the small number of lines observed at long wavelengths (small photon energies), and the increasing complexity of the spectrum at short wavelengths (high photon energies).

For the samples used in the experiments, the Fermi level at 4.2 K lies in the conduction band, at an energy of the order of 2 meV above the Γ_8 point. Photons of energies smaller than the Fermi energy can only induce intraband transitions, whereas photons of energies larger than the Fermi energy can also induce interband transitions between the Γ_8 bands.

In Figures 6, 7, and 8 we show the plots for the three experimental geometries of the positions in magnetic field of the minima of transmission

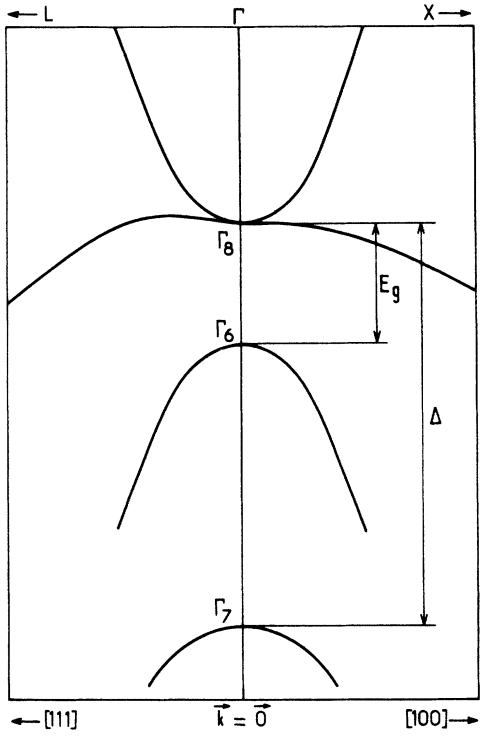

FIG. 1. Band structure of HgTe near $\vec{k}=0$.

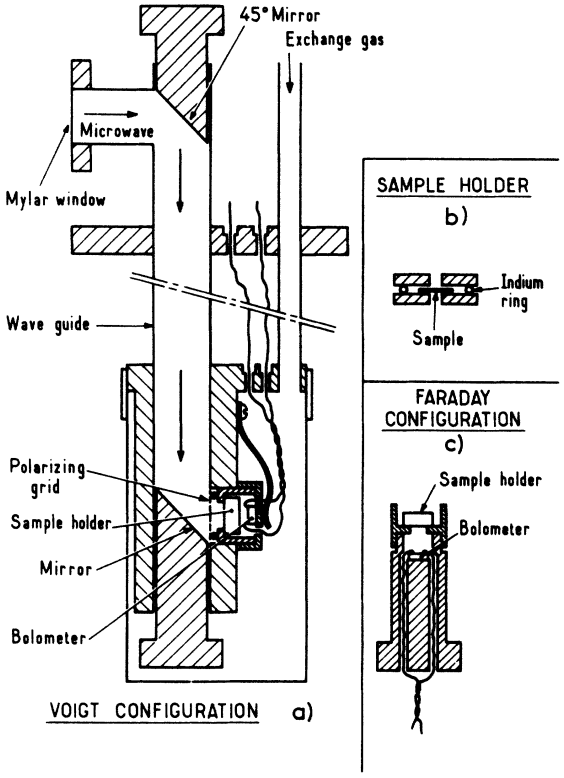

FIG. 2. Experimental arrangement: (a) waveguide arrangement providing the Voigt geometry in the vertical magnetic field of the coil; (b) sample holder; (c) this part replaces the bottom mirror in (a) to obtain the Faraday geometry.

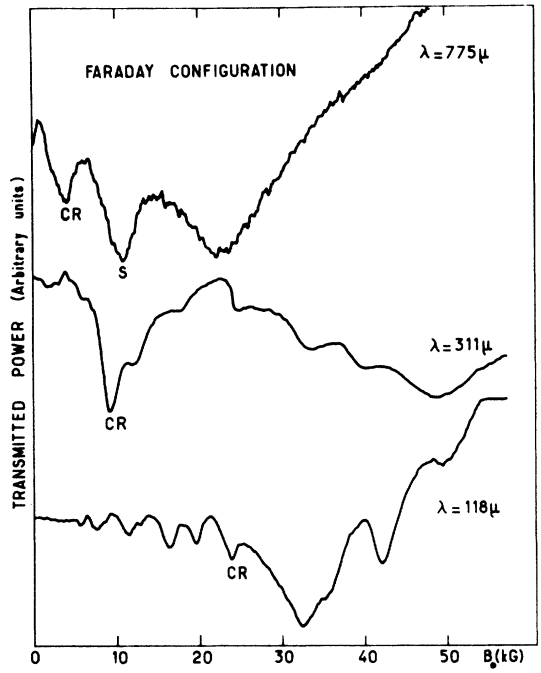

FIG. 3. Experimental recordings in the Faraday geometry at various wavelengths.

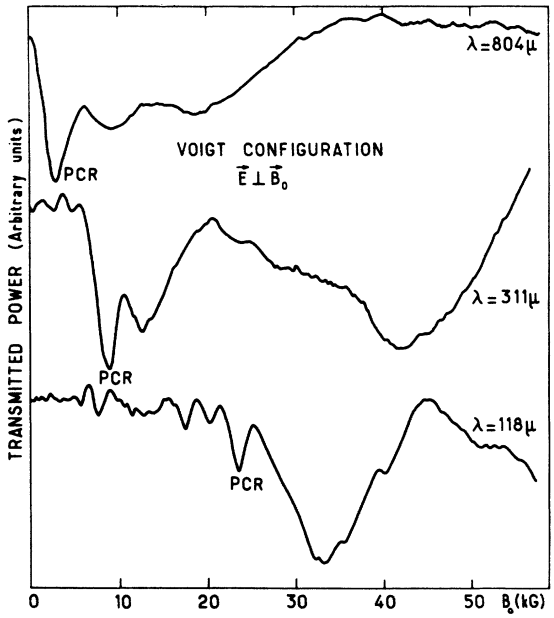

FIG. 4. Experimental recordings in the Voigt geometry ($\vec{E} \perp \vec{B}_0$) at various wavelengths.

versus the photon energies of the applied radiations.

A. Cyclotron Resonance and Plasma Cyclotron Resonance

If we compare the line labeled CR in the Faraday configuration (Fig. 6) and the line labeled PCR in the Voigt configuration (Fig. 7), we can see that their positions coincide at high energy and separate at low energy. This enables us to identi-

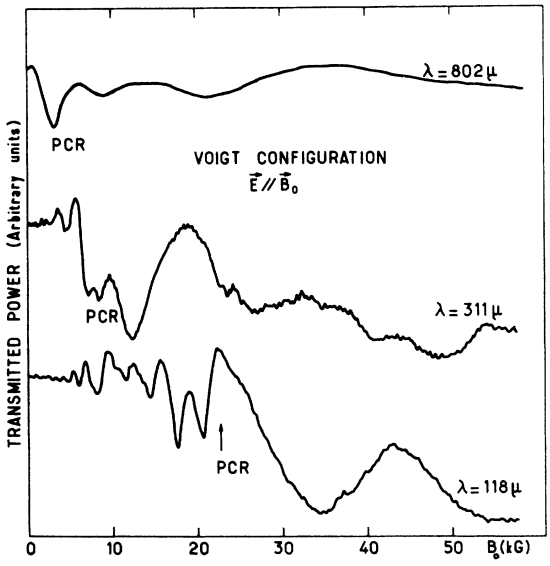

FIG. 5. Experimental recordings in the Voigt geometry ($\vec{E} \parallel \vec{B}_0$) at various wavelengths.

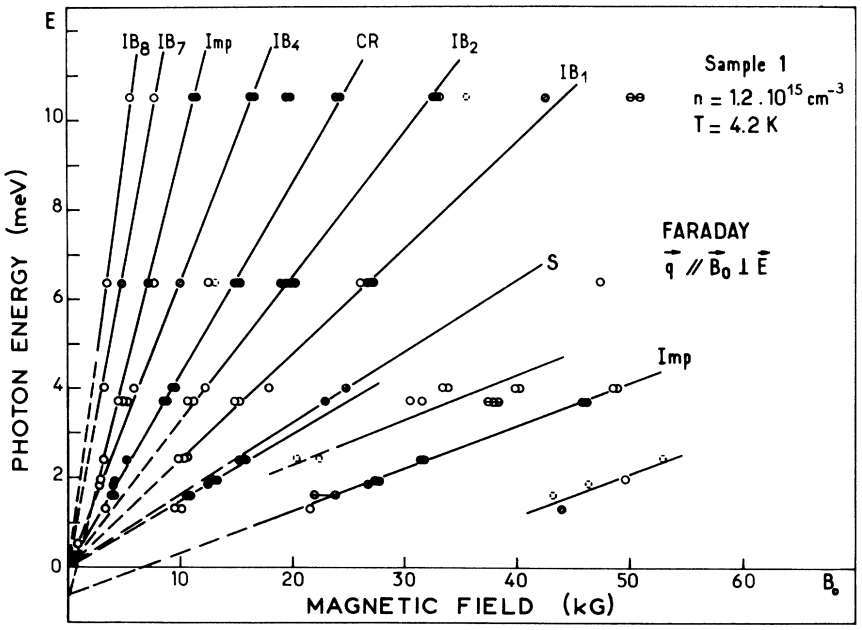

FIG. 6. Plot of the positions of the minima of transmitted power versus magnetic field for each applied photon energy in the Faraday geometry. •, strong absorption; O, weak absorption; ◌, very weak absorption.

fy these lines as the cyclotron resonance and the plasma-shifted cyclotron resonance in Faraday and Voigt geometries, respectively. This is confirmed by the fact that the corresponding absorption line is very weak in the Voigt geometry with $\vec{E} \parallel \vec{B}_0$.

In the Faraday geometry, the cyclotron-resonance absorption occurs at $\omega_c = \omega$. The corresponding transition energy $\Delta E = 4.35$ meV at $B_0 = 10$ kG, yields an apparent effective-mass value of $m_c^* = (0.026 \pm 0.001) m_0$. As we will show in Sec. III B, it is related to transitions between the quantum levels $\epsilon_1^-(1)$ and $\epsilon_1^-(2)$ labeled according to Luttinger.

In the Voigt geometry, the PCR line is shifted to lower magnetic fields if compared to the cyclotron-resonance line CR. In Fig. 9 we have plotted $E^2(B_0^2)$ for the PCR line for two samples. The position of the PCR line shows a parabolic dependence

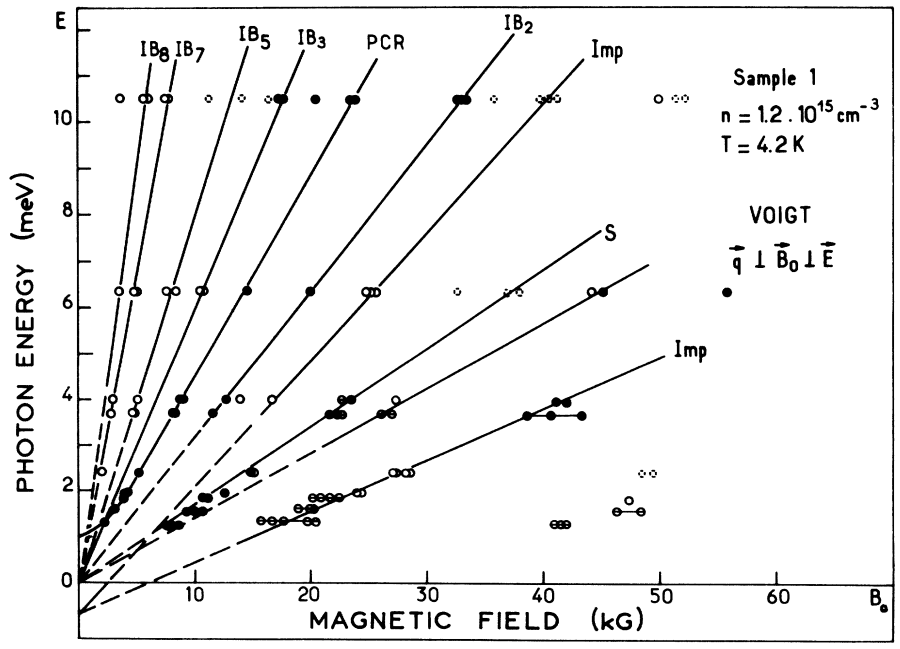

FIG. 7. Plot of the positions of the minima of transmitted power versus magnetic field for each applied photon energy in the Voigt geometry ($\vec{E} \perp \vec{B}_0$). •, strong absorption; O, weak absorption; ◌, very weak absorption.

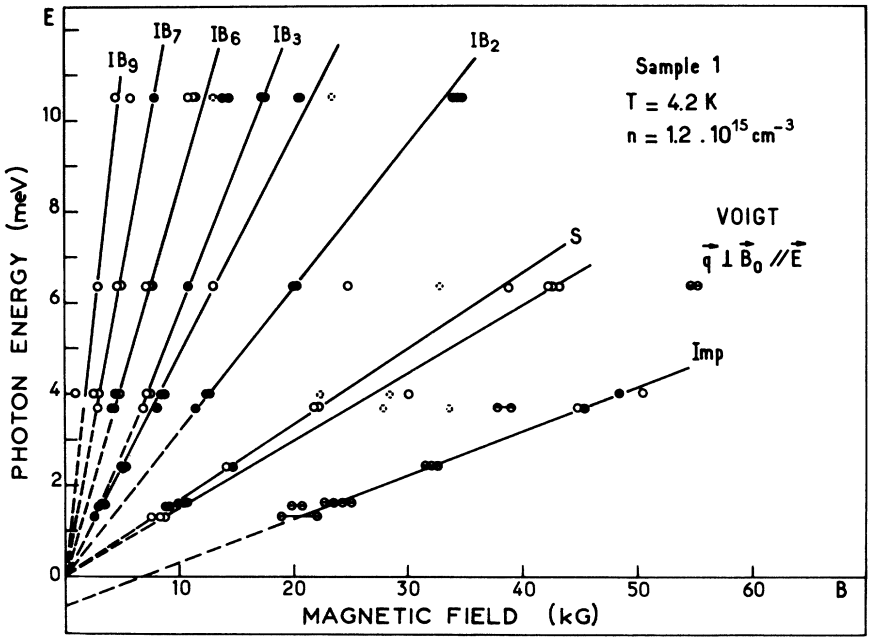

FIG. 8. Plot of the positions of the minima of transmitted power versus magnetic field for each applied photon energy in the Voigt geometry ($\vec{E} \parallel \vec{B}_0$). ●, strong absorption; O, weak absorption; □, very weak absorption.

on the magnetic field typical of a plasma-shifted cyclotron resonance. We recall that in Voigt geometry no absorption occurs at $\omega_c = \omega$. The carriers in cyclotron motion are coupled to one another by the depolarizing electric field. Furthermore, in a polar semiconductor, they are coupled to the polar LO phonons via the depolarizing electric field. This effect has been studied, for example, by Iwasa *et al.*[8] in indium antimonide. They have shown that a linearly polarized radiation, with the electric field perpendicular to the static magnetic field, interacts with the collective normal modes, which result from the mixing of the plasma-cyclotron-resonance mode at $\omega = (\omega_c^2 + \omega_p^2)^{1/2}$ with the polar LO phonons at ω_L.

In a zero-gap semiconductor, the propagation of an electromagnetic radiation is even more complicated. The standard procedure is to write down all the contributions to the dielectric function and look for solutions of the wave equation. As we use sample slabs of a thickness smaller than the wavelength, we will then have to calculate the transmission minima to obtain the observed position of the Voigt cyclotron resonance.

Grynberg, Le Toullec, and Balkanski[5] have calculated the dielectric function for mercury telluride in the local limit, and in the absence of magnetic field, for different electronic concentrations at different temperatures. The total dielectric function reads

$$\epsilon(\omega) = \epsilon'_\infty + \Delta\epsilon_{\text{inter}}^{\Gamma_8-\Gamma_8}(\omega) + \Delta\epsilon_{ph}(\omega) + \Delta\epsilon_{\text{intra}}^{\Gamma_8-\Gamma_8}(\omega) \ .$$

The interband transitions give rise, in a usual semiconductor, to the high-frequency contribution ϵ_∞ to the dielectric function. It is frequency independent in the region $\omega < E_g/\hbar$. Here it has been separated in the first two terms $\epsilon'_\infty + \Delta\epsilon_{\text{inter}}^{\Gamma_8-\Gamma_8}(\omega)$.

ϵ'_∞ is the high-frequency contribution to the dielectric function, which arises from the electronic transitions between all energy bands anywhere in the Brillouin zone, the $\Gamma_8 - \Gamma_8$ interband transitions

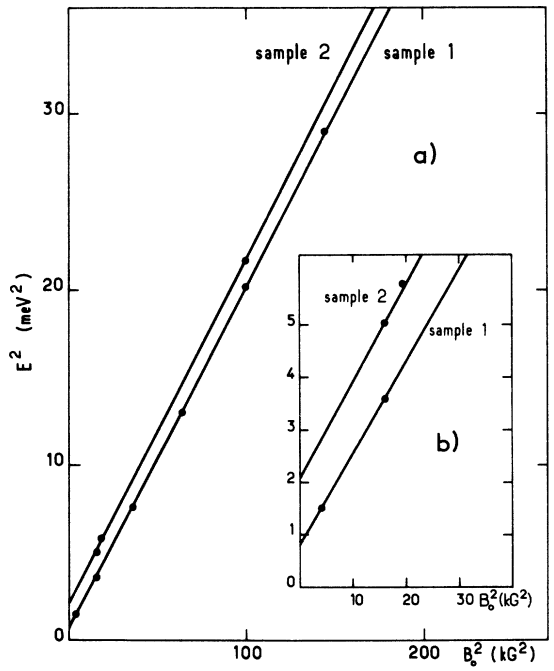

FIG. 9. Plot of the position of the P.C.R. line showing its dependence on B_0^2.

excepted.

$\Delta\epsilon_{\text{inter}}^{\Gamma_8\to\Gamma_8}(\omega)$ is the contribution arising from the $\Gamma_8 \to \Gamma_8$ interband transitions. Grynberg *et al.*[5] have shown that, at low temperature, this part depends strongly upon the frequency in the energy range where $\hbar\omega$, the photon energy, is of the order of the Fermi energy E_F.

$\Delta\epsilon_{ph}(\omega)$ is the contribution of the active phonon modes, and can be written under the general form

$$\Delta\epsilon_{ph}(\omega)=\sum_j \frac{F_j\omega_j}{\omega_j^2-\omega^2-i\Gamma_j\omega} \quad ,$$

where ω_j, F_j, and Γ_j are respectively the frequency, the oscillator strength and the damping parameters for the polar TO phonon modes. The authors of Ref. 5 have shown that there are two active modes. One of them corresponds to HgTe. The other may be connected with the possible existence of Hg_2Te.

$\Delta\epsilon_{\text{intra}}^{\Gamma_8\to\Gamma_8}(\omega)$ is the well-known contribution of the free carriers in the Γ_8 conduction band, i.e., the plasma term.

$\Delta\epsilon_{\text{inter}}^{\Gamma_8\to\Gamma_8}(\omega)$ consists of a real and an imaginary part related by Kramers-Kronig relations:

$$\Delta\epsilon_{\text{inter}}^{\Gamma_8\to\Gamma_8}(\omega)=\Delta\epsilon'(\omega)+i\Delta\epsilon''(\omega) \quad .$$

Neglecting the effects of nonparabolicity and the warping of the Γ_8 bands, Grynberg *et al.*[5] obtain, in the random-phase approximation,

$$\Delta\epsilon'(\omega)=A\left\{\left(\frac{1}{\hbar\omega}\right)^{1/2}\times\left[\left(1+\exp\left(-\frac{E_F}{kT}\right)\right)^{-1}\left(1+\exp\left(\frac{E_F+\hbar\omega}{kT}\right)\right)^{-1}-\left(1+\exp\left(\frac{E_F}{kT}\right)\right)^{-1}\left(1+\exp\left(\frac{-E_F-\hbar\omega}{kT}\right)\right)^{-1}\right]+\sum_{\nu=0}^{\infty}\frac{4kT(E_F^2+P_\nu^2)^{1/4}\sin(\Theta_\nu-\frac{1}{2}\Phi_\nu)}{[(E_F^2+\hbar^2\omega^2-P_\nu^2)^2+4E_F^2P_\nu^2]^{1/2}}\right\}$$

and

$$\Delta\epsilon''(\omega)=A\left(\frac{1}{\hbar\omega}\right)^{1/2}\times\left\{\left[1+\exp\left(-\frac{E_F}{kT}\right)\right]^{-1}\left[1+\exp\left(\frac{E_F-\hbar\omega}{kT}\right)\right]^{-1}-\left[1+\exp\left(\frac{E_F}{kT}\right)\right]^{-1}\left[1+\exp\left(\frac{-E_F+\hbar\omega}{kT}\right)\right]^{-1}\right\}$$

where

$$A=2\left(\frac{m_0e^4}{2\hbar^2}\right)^{1/2}\left(\frac{m_c^*}{m_0}\right)^{1/2} \quad ,$$

$$P_\nu=kT\pi(2\nu+1) \quad ,$$

$$\tan\Theta_\nu=\frac{2E_FP_\nu}{E_F^2+\hbar^2\omega^2-P_\nu^2} \quad ,$$

and

$$\tan\Phi_\nu=\frac{P_\nu}{E_F} \quad .$$

In the presence of an external magnetic field, one must take into account the dependence of the dielectric function upon magnetic field.

The contributions ϵ_∞' and $\Delta\epsilon_{ph}(\omega)$ do not depend on the magnetic field. In our experiments, the shift of the plasma cyclotron resonance is important only at low frequency, with magnetic fields smaller than 6 kG. For this range of magnetic fields we can neglect the quantization of the Γ_8 bands. In this case, the Fermi energy does not vary with magnetic field and the contribution $\Delta\epsilon_{\text{inter}}^{\Gamma_8\to\Gamma_8}(\omega)$ does not depend on the magnetic field. Finally, we introduce classically the magnetic field in the plasma term, which we write in the Drude-Zener approximation of an energy-independent relaxation time. The frequency- and magnetic-field-dependent dielectric function reads

$$\epsilon(\omega,B_0)=\epsilon_\infty'+\Delta\epsilon_{\text{inter}}^{\Gamma_8\to\Gamma_8}(\omega)+\Delta\epsilon_{ph}(\omega)+\Delta\epsilon_{\text{intra}}^{\Gamma_8\to\Gamma_8}(\omega,B_0) \quad .$$

Then in the Voigt configuration, the normal mode of wave propagation leading to plasma cyclotron resonance is given by

$$\epsilon_\perp=\epsilon_{xx}+\epsilon_{xy}^2/\epsilon_{xx}=\epsilon_+\epsilon_-/\epsilon_{xx} \quad ,$$

where

$$\epsilon_\pm=\epsilon_{xx}\pm i\epsilon_{xy} \quad .$$

We have

$$\epsilon_\pm(\omega,B_0)=\epsilon_\infty'+\Delta\epsilon_{\text{inter}}^{\Gamma_8\to\Gamma_8}(\omega)+\Delta\epsilon_{ph}(\omega)+i\frac{\omega_p^2}{\omega}\frac{\tau}{1-i(\omega\pm\omega_c)\tau}$$

and

$$\epsilon_{xx}(\omega,B_0)=\epsilon_\infty'+\Delta\epsilon_{\text{inter}}^{\Gamma_8\to\Gamma_8}(\omega)+\Delta\epsilon_{ph}(\omega)+i\frac{\omega_p^2}{\omega}\frac{\tau(1-i\omega\tau)}{(1-i\omega\tau)^2+(\omega_c\tau)^2} \quad .$$

Here ω_p^2 is the quantity

$$\omega_p^2=ne^2/m_c^*\epsilon_0 \quad .$$

n and m_c^* are the free-carrier concentration and effective mass, respectively, τ is the momentum relaxation time, ω_c is the cyclotron frequency, and ϵ_0 is the permittivity of free space.

The real and imaginary parts of $\epsilon_\perp$ can be written

$$\text{Re}(\epsilon_\perp)=\frac{[(A_+A_-)-(B_+B_-)]\,\text{Re}\,\epsilon_{xx}+[(A_+B_-)+(A_-B_+)]\text{Im}\epsilon_{xx}}{(\text{Re}\,\epsilon_{xx})^2+(\text{Im}\,\epsilon_{xx})^2},$$

$$\text{Im}(\epsilon_\perp)=\frac{[(A_+B_-)+(A_-B_+)]\,\text{Re}\,\epsilon_{xx}-[(A_+A_-)-(B_+B_-)]\,\text{Im}\,\epsilon_{xx}}{(\text{Re}\,\epsilon_{xx})^2+(\text{Im}\,\epsilon_{xx})^2},$$

where

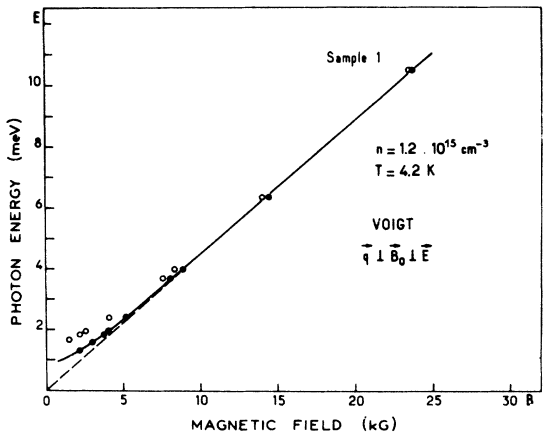

FIG. 10. Experimental and calculated magnetic field dependence of the P.C.R. Full dots, experimental positions; solid line, calculated positions; open circles, calculated position neglecting the frequency dependence of the dielectric contribution due to the interband $\Gamma_8 \rightarrow \Gamma_8$ transitions and making $\epsilon'_\infty + \Delta\epsilon^{\Gamma_8 \rightarrow \Gamma_8}_{\text{inter}}(\omega) = 20\epsilon_0$.

$$A_\pm = \epsilon'_\infty + \mathrm{Re}\,(\Delta\epsilon^{\Gamma_8 \rightarrow \Gamma_8}_{\text{inter}}(\omega) + \Delta\epsilon_{\text{ph}}(\omega)) - \frac{\omega_p^2}{\omega}\frac{\tau^2(\omega \pm \omega_c)}{1+\tau^2(\omega \pm \omega_c)^2} ,$$

$$B_\pm = \mathrm{Im}\,(\Delta\epsilon^{\Gamma_8 \rightarrow \Gamma_8}_{\text{inter}} + \Delta\epsilon_{\text{ph}}) + \frac{\omega_p^2}{\omega}\frac{\tau}{1+\tau^2(\omega \pm \omega_c)^2} .$$

From this we calculate the transmission coefficient T through the sample as a function of the magnetic field. The general formula which takes into account multiple reflections and interference phenomena is

$$T = e^{-\alpha d}\left(\frac{(1-R)^2 + 4R^2\sin\Phi_r}{(1-Re^{-\alpha d})^2 + 4Re^{-\alpha d}\sin^2[(\omega/c)nd + \Phi_r]}\right) ,$$

with

$$\tan\Phi_r = \frac{2k}{1-n^2-k^2}$$

where α is the absorption coefficient, d is the sample thickness, n is the index of refraction, k is the extinction coefficient, and R is the reflection coefficient.

The transmission is computed numerically as a function of magnetic field for different energies. The value of the effective mass used in the calculation is the cyclotron mass determined in the Faraday configuration, and the other parameters such as ϵ'_∞, ω_j, F_j, Γ_j are taken from the work of Grynberg *et al.* The only adjustable parameter is the electronic concentration n. For sample No. 1 we obtain $n = 1.2\times10^{15}$ cm^{-3} and for sample No. 2, $n = 2\times10^{15}$ cm^{-3}. In Fig. 10 the calculated position is compared with the experimental position for sample No. 1. [For the sake of comparison, we have plotted in Fig. 10 the calculated position obtained when supposing that the comtribution of the $\Gamma_8 \rightarrow \Gamma_8$ interband transitions is constant, and allowing $\epsilon'_\infty + \Delta\epsilon^{\Gamma_8 \rightarrow \Gamma_8}_{\text{inter}} = 20\epsilon_0$ and $n = 1.2\times10^{15}$ cm^{-3} (open circles). The discrepancy with the experimental results is evident.]

B. Intraband and Interband Transitions

The quantum energy levels, in both the conduction and the valence bands near the Γ_8 point, are determined by a set of five parameters introduced by Luttinger.[1] The problem is therefore to find the set which fits, at the same time, the $\Gamma_8 \rightarrow \Gamma_8$ intraband transitions and the $\Gamma_8 \rightarrow \Gamma_8$ interband transitions. Futhermore, this set of parameters must also fit the interband $\Gamma_6 \rightarrow \Gamma_8$ transitions observed by Guldner, Rigaux, Mycielski, and Grynberg[9] on samples similar to ours, in their magnetotransmission experiments in the infrared region (see preceding paper). In our energy range, the effects of nonparabolicity are negligible. Following Groves, Brown, and Pidgeon,[10] we neglect the possible existence of $\vec{k}$ linear terms in the Γ_8 valence band. Furthermore, Laewetz[11] has shown by a semiphenomenological calculation that the warping of the Γ_8 bands is negligible. The energy separation between the Γ_7 and the Γ_8 bands is very large: $\Delta \sim 1$ eV. Therefore, we also neglect the direct influence of the spin-orbit interaction on the Γ_8 bands. Under these simplifying assumptions the quantum levels in the Γ_8 bands fall into two sets, corresponding to $m_J = +\frac{3}{2}, -\frac{1}{2}$ and $m_J = +\frac{1}{2}, -\frac{3}{2}$, respectively. They are given according to Ref. 1 by:

$$\epsilon_1(0) = \tfrac{1}{2}(\gamma_1 - \bar{\gamma}) - \tfrac{1}{2}\kappa, \quad \epsilon_1(1) = \tfrac{3}{2}(\gamma_1 - \bar{\gamma}) - \tfrac{1}{2}\kappa ,$$

$$\epsilon_1^\pm(n) = \gamma_1 n - (\tfrac{1}{2}\gamma_1 + \bar{\gamma} - \tfrac{1}{2}\kappa) \pm \{[\bar{\gamma}n - (\gamma_1 - \kappa + \tfrac{1}{2}\bar{\gamma})]^2 + 3\bar{\gamma}^2 n(n-1)\}^{1/2} \quad \text{for } n \geq 2;$$

$$\epsilon_2(0) = \tfrac{1}{2}(\gamma_1 + \bar{\gamma}) - \tfrac{3}{2}\kappa, \quad \epsilon_2(1) = \tfrac{3}{2}(\gamma_1 + \bar{\gamma}) - \tfrac{3}{2}\kappa ,$$

$$\epsilon_2^\pm(n) = \gamma_1 n - (\tfrac{1}{2}\gamma_1 - \bar{\gamma} + \tfrac{1}{2}\kappa) \pm \{[\bar{\gamma}n + (\gamma_1 - \kappa - \tfrac{1}{2}\gamma_1)]^2 + 3\bar{\gamma}^2 n(n-1)\}^{1/2} \quad \text{for } n \geq 2$$

The plus sign corresponds to the holes and the minus sign to the electrons. The levels $\epsilon_1(0)$, $\epsilon_1(1)$, $\epsilon_2(0)$, and $\epsilon_2(1)$ are the levels $\epsilon_1^+(n)$ and $\epsilon_2^+(n)$ for $n = 0, 1$. The transitions favored by the selection rules are the following:

(i) inside a given set of levels the transitions with $\Delta n = \pm 1$ (i.e., cyclotron resonance); (ii) from one set to the other, transitions with $\Delta n = 0$ (we shall note these $\Delta s = \pm 1$, because at high quantum number they would correspond to spin transitions); (iii) interband transitions with $\Delta n = \pm 1$ in the same set of levels.

The best agreement between the experimental and the calculated energies of the transitions is

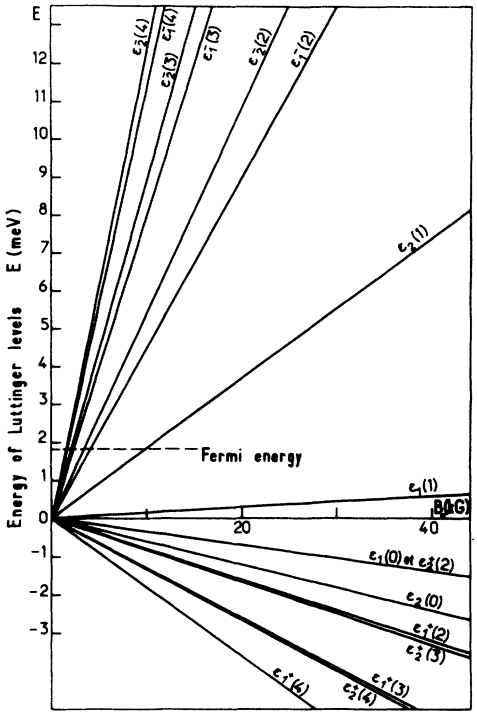

FIG. 11. Scheme of the calculated Luttinger levels versus magnetic field.

obtained with the following values of the parameters:

$\bar{\gamma} = -8.3 \pm 0.2$; $\gamma_1 = -12.8 \pm 0.6$; $\kappa = -10.5 \pm 0.4$.

In Fig. 11 the calculated energy levels are shown as a function of B_0. We can attribute all the observed absorption lines to definite transitions. A summary of the experimental and calculated values of the energies of the transitions in the Faraday geometry is given in Table I and Fig. 12, with the corresponding selection rules. One line labeled IB_2 corresponds to $\Delta n = -3$. This selection rule can be explained if warping and $\vec{k}$ linear terms are included. It may also arise from impurities, rather than from interband transitions. One can see that at high photon energy the "combined $\Delta n = 1$, $\Delta s = 1$ resonance" is observed.

C. Impurity Levels

In Figs. 6, 7, and 8 we observe one line labeled Imp, which appears for magnetic fields larger than 20 kG and which extrapolates for zero magnetic field at a negative energy of the order of 0.7 meV. We tentatively attribute this line to transitions from an impurity level which lies in the conduction band, to one of the quantum levels which has an energy larger than the Fermi energy.

In a zero-gap semiconductor, an acceptor level is degenerate with the conduction-band continuum. In first approximation, the wave function of the acceptor is constructed from valence-band wave functions, with some mixing of conduction-band wave functions because of the degeneracy at Γ_8 at $\vec{k} = 0$. Therefore, an acceptor impurity can create discrete levels for the ground state and the excited states, because of the heavy effective mass of the valence band. On the contrary, a donor impurity cannot create discrete levels, which would be degenerated with the valence-band continuum, because of the light effective mass of the conduction

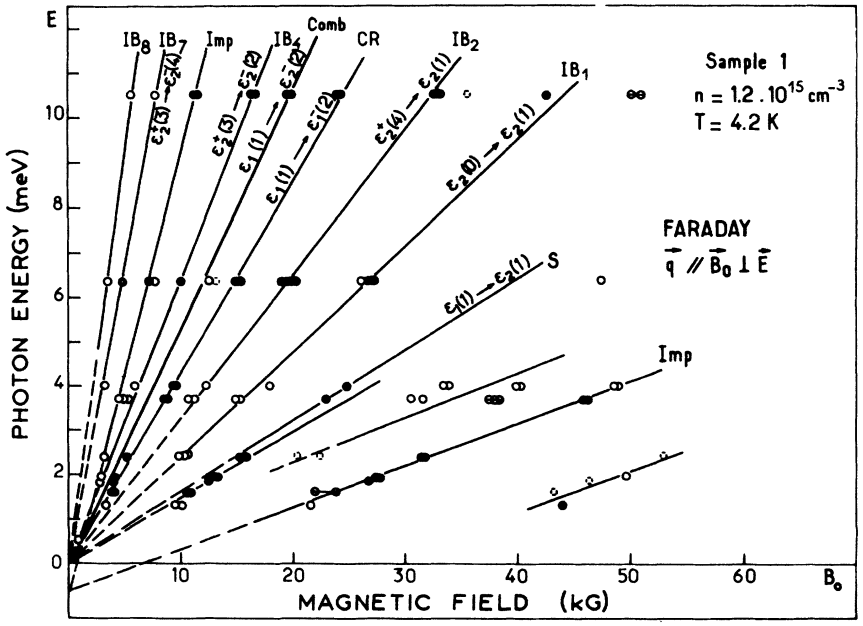

FIG. 12. Absorptions and corresponding transitions in the Faraday geometry.

TABLE I. Experimental absorptions and corresponding transitions in the Faraday geometry. Comparison between the observed and the calculated energies of the transitions.

Name	Experimental slope meV/10 kG	Transition	Calculated slope meV/10 kG	Error	Selection rules
S	1.65	$\epsilon_1(1) \rightarrow \epsilon_2(1)$	1.7	3%	$\Delta n = 0,\ \Delta s = 1$
IB_1	2.40	$\epsilon_2(0) \rightarrow \epsilon_2(1)$	2.40	···	$\Delta n = 1,\ \Delta s = 0$
IB_2	3.25	$\epsilon_2^+(4) \rightarrow \epsilon_2(1)$	3.15	3%	$\Delta n = -3,\ \Delta s = 0$
CR	4.35	$\epsilon_1(1) \rightarrow \epsilon_1^-(2)$	4.35	···	$\Delta n = 1,\ \Delta s = 0$
COMB	5.05	$\epsilon_1(1) \rightarrow \epsilon_2^-(2)$	5.25	4%	$\Delta n = 1,\ \Delta s = 1$
IB_4	6.35	$\epsilon_2^+(3) \rightarrow \epsilon_2^-(2)$	6.25	2%	$\Delta n = -1,\ \Delta s = 0$
IB_7	13.2	$\epsilon_2^+(3) \rightarrow \epsilon_2^-(4)$	13.2	···	$\Delta n = 1,\ \Delta s = 0$

band.

For magnetic fields larger than 20 kG, the impurity level lies under all the quantum levels of the conduction band except the level $\epsilon_1(1)$. The absorption line corresponds to the transition of electrons from the impurity level to one of the empty levels of the conduction band.

IV. DISCUSSION

In Fig. 11 one can see that at high quantum number $n > 3$ the levels of each set in the conduction and valence bands become evenly spaced. Thus one can define an effective mass and a Landé factor. For instance, we have

$$\epsilon_1^-(4) - \epsilon_1^-(3) = \epsilon_2^-(4) - \epsilon_2^-(3) = 3.45 \text{ meV}$$

at 10 kG and around 12 meV.

From this we obtain

$$m_c^* \ (n > 3,\ E \sim 12 \text{ meV}) = 0.034 m_0 \ .$$

In the same way, we have

$$\epsilon_2^-(4) - \epsilon_1^-(4) = \epsilon_2^-(3) - \epsilon_1^-(3) = 1 \text{ meV}$$

at 10 kG and around 12 meV. Then we obtain

$$g_c^* \ (n > 3,\ E \sim 12 \text{ meV}) = -17.3 \ .$$

For the valence band we obtain

$$m_v^* \ (E = 1 \text{ meV}) = 0.24 m_0 \text{ and } g_v^* \ (E = 1 \text{ meV}) = -8$$

at 10 kG and 1 meV.

Guldner *et al.*[9] have adjusted the $\Gamma_6 \rightarrow \Gamma_8$ transitions in the high-energy region, where there are no quantum effects. They used the nonparabolic model of Kane applied by Kacman and Zawadzki[12] to the zero-gap semiconductors. They obtained the band-edge values for the Γ_8 conduction band:

$$m_c^* \ (E = 0) = (0.031 \pm 0.001) m_0 \ ,$$

$$g_c^* \ (E = 0) = -22 \pm 4 \ .$$

These values are fitting parameters and cannot be experimentally observed because of the Luttinger effect. From these values one can calculate the effective mass at a given energy E in the conduction band, taking into account the effects of nonparabolicity:

$$m_c^* \ (E) = m_c^* \ (E = 0)(1 + 2E/E_g) \ ,$$

where E_g is the energy separation between the Γ_6 and Γ_8 levels.

One obtains $m_c^* \ (E = 12 \text{ meV}) = 0.033 m_0$, in very good agreement with the value taken from the Luttinger levels, in an energy range where nonparabolicity is almost negligible. At the same energy, the value of the Lande factor should be smaller than it is at the bottom of the band. One should obtain $g_c^* \ (E = 12 \text{ meV}) \sim -20$, in agreement with the value obtained from the Luttinger theory. In order to discuss further the validity of our parameters, we have tried to compare them with the experimental data of other workers on the Γ_8 conduction band.

Stradling and Antcliffe[13] have studied the temperature dependence of the quantum oscillations of magnetoresistance in samples of concentration $n = 2 \times 10^{15}$ cm^{-3}. They obtain $m_c^* = (0.029 \pm 0.003) m_0$. This value obviously corresponds to a mean value between the apparent effective mass $m_c^* = 0.026 m_0$ corresponding to the transition $\epsilon_1^-(1) \rightarrow \epsilon_1^-(2)$, and the value $0.034 m_0$ obtained from the high-quantum-number levels which are evenly spaced.

Tsidilkovski and Ponomarev[14] and Bashirov and Gadzhieva[15] have studied the positions of the maxima of the first Shubnikov-de Haas ocillations, which only give the product $|g^*| m^*$, and therefore are difficult to analyze. Saleh and Fan[16] have studied the magneto-optical-absorption transitions in the 3.5–35μm range. From the separation of the $n = 3$ level they obtain $|g_c^*| = 19 \pm 3$.

In order to test the quality of our parameters we proceed as follows. We first estimate the energy E of the quantum levels involved in each experiment. Then we calculate the effective mass at E using the above formula with the band-edge mass $m_c^* \ (E = 0 \text{ meV}) = 0.031 m_0$. Using the formula given by Kacman and Zawadzki,[12] we finally calculate the Landé factor by

TABLE II. Cyclotron mass and Landé factor in the conduction band. Comparison between the experimental values found by other workers and the calculated values of m_c^* and g_c^*, using our values of the Luttinger parameters and taking into account the corrections due to the energy of the levels involved in each of these experiments.

	Quantum number of level involved	Energy E of quantum level involved (in meV)	Calculated values with our parameters $m_c^*(E)/m_0$	$\lvert g_c^*(E)\rvert$	Experimental values $m_c^*(E)/m_0$	$\lvert g_c^*(E)\rvert$
Stradling and Antcliffe	...	2.2	0.031	29	0.029	...
Tsidilkovski and Ponomarev	$n=1$	36.1	0.038	22	...	$19 < \lvert g_c \rvert < 29$
Bashirov and Gadzhieva	$n=1$	58.4	0.043	18.5	...	17
Saleh and Fan	$n=3$	46	0.040	20.3	0.028	19

$$g^*(E) = 2\left[1 - \left(\frac{m_0}{m_0^*(E)} - 1\right)\left(\frac{\Delta}{3E+2\Delta}\right)\right]$$

This formula is only valid for high energies and high quantum numbers. E is the energy taken from the top of the valence band, and Δ is the spin-orbit interaction energy. The results of the comparisons between experiment and theory are summarized in Table II.

In conclusion, it seems that most of the experimental results can be interpreted with the given parameters, if one takes into account the Luttinger effect for the levels of low quantum numbers and the nonparabolicity effects for energies larger than 40 meV.

As for the impurity states, we may add the following. Finck *et al.*[17] have studied the mobility as a function of temperature in mercury telluride samples of low electronic concentration. They observe two minima of the mobility, which they attribute to a resonant scattering when the Fermi energy is equal to the activation energy of the acceptor level. They find two acceptor states corresponding to the activation energies $E_{A_1} = 2.25$ meV and $E_{A_2} = 9.5$ meV. The same effect has been observed by Ivanov-Omskii *et al.*[18] Furthermore, Finck *et al.*[17] observe a systematic decrease of the mobility at temperatures lower than 2 K, and suggest that this could be due to a resonant scattering on copper occurring at $T < 1.5$ K. Sologub *et al.*[19] have performed measurements down to 0.05 K, and observe a mobility anomaly around 1 K which could have the same origin. The corresponding acceptor state lies at an energy of the order of $E_A \sim 0.8 \pm 0.2$ meV. It is probably this state that we observe. On the other hand, Gel'mont and D'yakonov[6] have calculated the ionization energy for the ground state of an acceptor, in the hydrogenoid approximation in the absence of magnetic field. This model could apply for instance to acceptor states arising from mercury vacancies. They find about 6 meV and a half-width of the order of 1.2 meV. In this model the impurity level that we observe at 0.7 meV above the Γ_8 point would correspond to one of the excited states of the impurity. The electric concentration $n \sim 2 \times 10^{15}$ cm^{-3} observed in these samples at 4.2 K is of the order of magnitude of what it would be in intrinsic crystals. Since we observe acceptor states there must also exist donor impurities for compensation. These donor impurities have energies degenerate with the valence band but do not lead to discrete observable levels.

V. SUMMARY AND CONCLUSIONS

We have performed the first observation of cyclotron resonance in HgTe. To interpret the position of the plasma-shifted cyclotron resonance in the geometry of Voigt, we have taken into account the frequency-dependent contribution of the $\Gamma_8 \rightarrow \Gamma_8$ interband transitions to the dielectric constant, and introduced classically the magnetic field in the plasma term. The result of the calculation is in excellent agreement with the experimental results. The interpretation of the absorption lines due to intraband and interband transitions leads us to the determination of the Luttinger parameters, which describe the quantum energy levels of both Γ_8 bands in a magnetic field near the degeneracy point at Γ_8. This determination was made much easier by a constant comparison with the results of the magnetotransmission experiments reported in the preceding paper. Finally, we have also observed transitions between a discrete acceptor state and the quantum levels of the conduction band.

ACKNOWLEDGMENTS

We are greatly indebted to Professor J. Bok and to our colleagues at E.N.S., Dr. C. Rigaux and Dr. Y. Guldner, for many stimulating and enlightening discussions. One of us (M. G.) wishes to thank D.G.R.S.T. for their invitation and financial support and Professor M. Balkanski for giving him the possibility of working in the Laboratoire de Physique des Solides de l'Université Paris VI.

*On leave from the Institute of Experimental Physics, Warsaw University, Warsaw, Poland.
†Laboratoire de Physique des Solides de l'Université Paris VI, 9 quai St. Bernard, Paris Ve, France.

[1]J. M. Luttinger Phys. Rev. **102,** 1030 (1956).
[2]R. C. Fletcher, W. A. Yager, and F. R. Merritt, Phys. Rev. **100,** 747 (1955)
[3]D. Sherrington and W. Kohn, Phys. Rev. Lett. **21,** 153 (1968).
[4]J. G. Broerman, Phys. Rev. B **5,** 397 (1972).
[5]M. Grynberg, R. Le Toullec, and M. Balkanski, Phys. Rev. B (to be published).
[6]B. L. Gel'mont and M. I. D'Yakonov, Zh. Eksp. Teor. Fiz. **62,** 713 (1972) [Sov. Phys.-JETP **35,** 377 (1972)].
[7]P. N. Robson in *Coherent Sources using Electron Beams. Spectroscopic Techniques*, edited by D. H. Martin (North-Holland, Amsterdam, 1967), p. 261.
[8]S. Iwasa, Y. Sawada, E. Burstein, and E. D. Palik. J. Phys. Soc. Jap. Suppl. **21,** 742 (1966).
[9]Y. Guldner, C. Rigaux, and Mycielski, and M. Grynberg, preceding paper, Phys. Rev. B 8, 3875 (1973).
[10]S. H. Groves, R. N. Brown, and C. R. Pidgeon, Phys. Rev. **161,** 779 (1967).
[11]P. Laewetz, Phys. Rev. B **4,** 3460 (1971).
[12]P. Kacman and W. Zawadzki Phys. Status Solidi **47,** 629 (1971).
[13]R. A. Stradling and G. A. Antcliffe, J. Phys. Soc. Jap. Suppl. **21,** 374 (1966).
[14]I. M. Tsidilkovski and A. I. Ponomarev, in *Proceedings of the International Conferencc on II-VI Semiconducting Compounds,* edited by D. G. Thomas (Benjamin, New York, 1967), p. 1080.
[15]R. I. Bashirov and R. M. Gadzhieva, Fiz. Tekh. Poloprovodn **4,** 1936 (1970) [Sov. Phys.-Semicond. **4,** 1659 (1971)].
[16]A. S. Saleh and H. Y. Fan, Phys. Status Solidi **53,** 163 (1972).
[17]C. Finck, S. Otmezguine, G. Weill, and C. Verie, in *Proceedings of the Eleventh International Conference on the Physics of Semiconductors* (PWN-Polish Scientific Publishers, Warsaw, 1972), p. 944.
[18]V. I. Ivanov-Omskii, B. T. Kolomiets, V. K. Ogorodnikov, and K. P. Smekalova, Fiz. Tekh. Poloprovodn **4,** 264 (1970) [Sov. Phys.-Semicond. **4,** 214 (1970)].
[19]V. V. Sologub, V. I. Ivanov-Omskii, V. M. Muzhdaba, and S. S. Shalyt, Fiz. Tverd. Tela **13,** 1738 (1971) [Sov. Phys.-Solid State **13,** 1452 (1971)].